IUCrJ

Volume 9 (2022)

Supporting information for article:

Real-space texture and pole-figure analysis using the 3D pair distribution function on a platinum thin film

Sani Y. Harouna-Mayer, Songsheng Tao, ZiZhou Gong, Martin v. Zimmermann, Dorota Koziej, Ann-Christin Dippel and Simon J. L. Billinge

9. Supporting Information

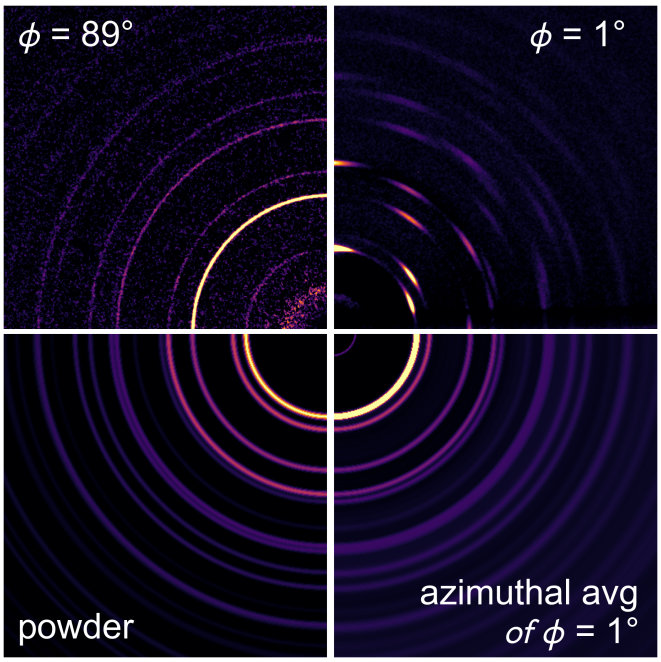

Fig. S.1. Sections of detector images of the textured Pt sample at tilt angles $\phi = 1°$ and $\phi = 89°$ and the detector image averaged over the azimuth of the $\phi = 1°$ dataset, and a simulated perfect powder Pt detector image. The colorscale is in arbitrary units and the relative intensities of the lines are the most important. This shows that azimuthally averaging the intensity of the 1° diffraction images results in a diffraction pattern that is much closer to that of the powder than obtained for the 89° angle image.

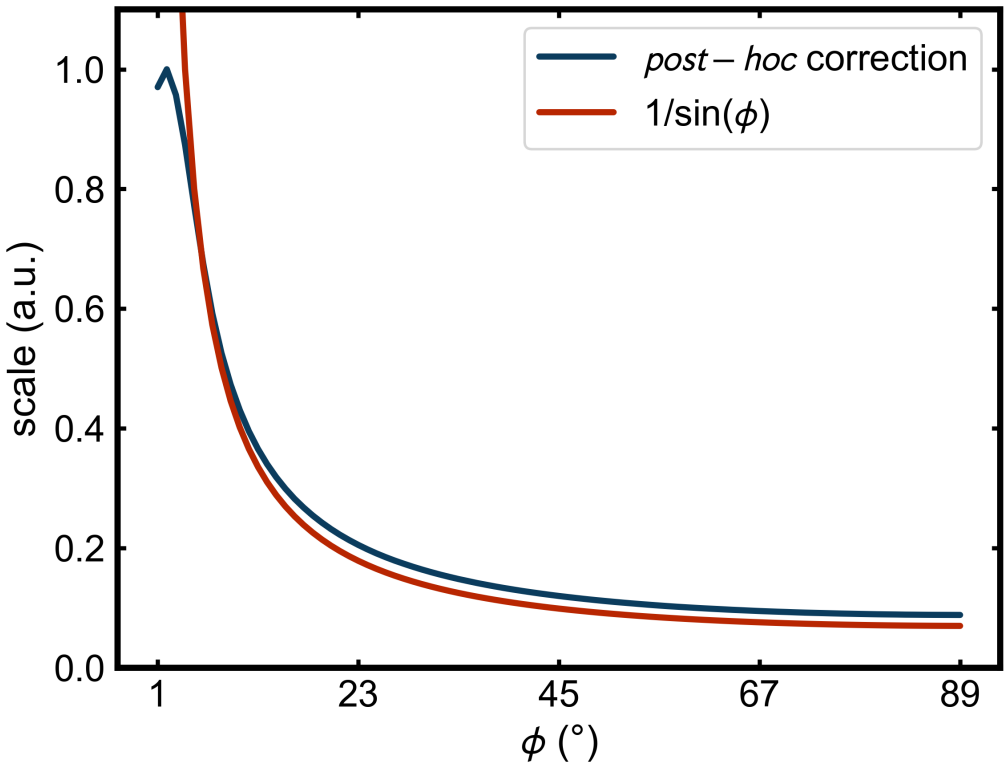

Fig. S.2. *Post-hoc* correction versus mathematical correction for the intensity scaling of the diffraction images and patterns taking into account the different illuminated volumes of the sample at different tilt angles ϕ.

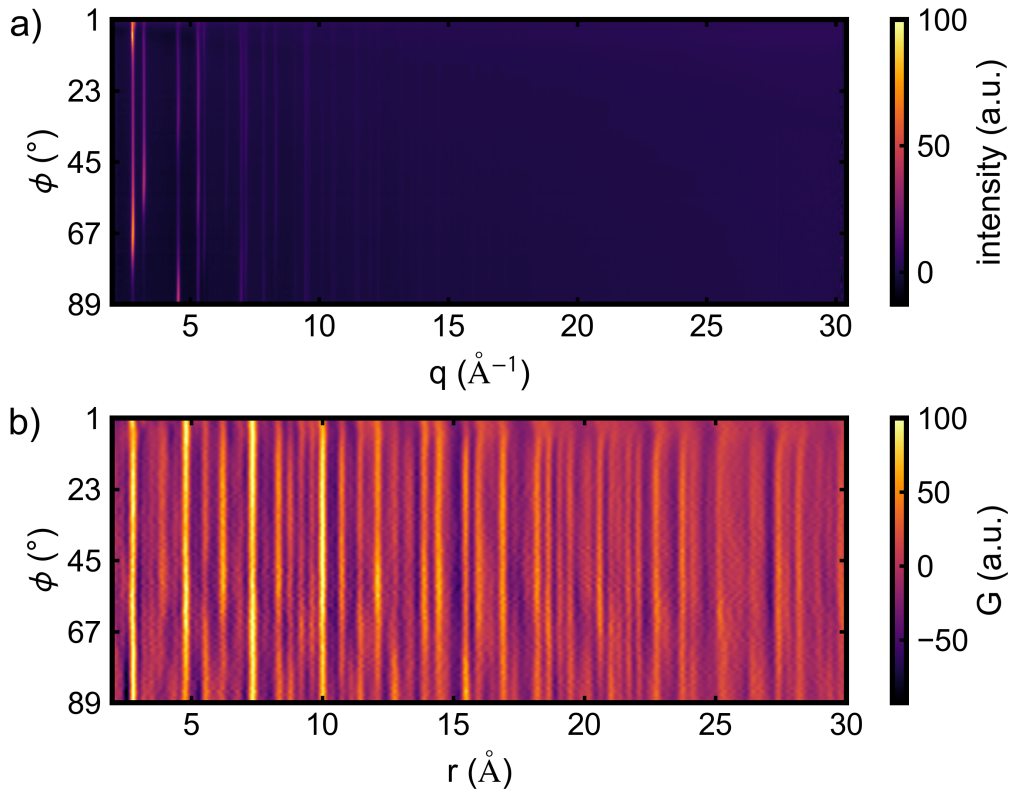

Fig. S.3. a) 1D XRD and b) 1D PDF from the Pt thin film at different tilt angles ϕ.

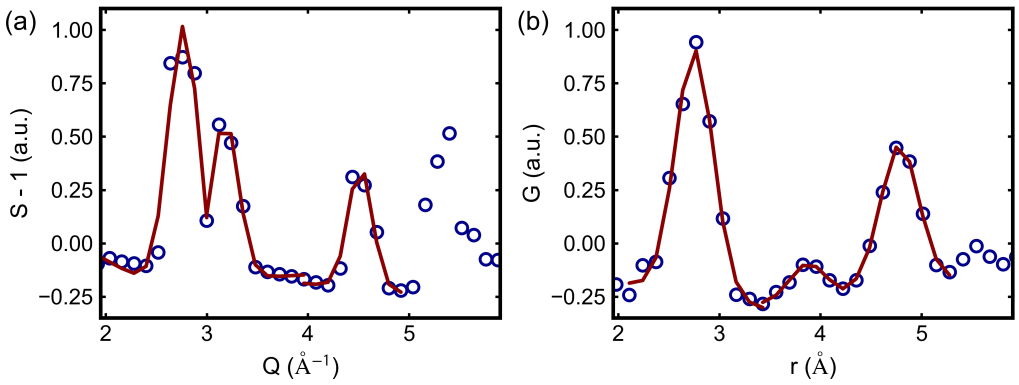

Fig. S.4. Gaussian fits of the first three peaks in the spherical integration of (a) the total scattering structure function $S(\mathbf{Q}) - 1$ and (b) the txPDF $G(\mathbf{r})$. The fit results of the FWHMs are listed in table S.1 and S.2. The peaks at higher Q/r are not shown due to a poor fit quality because of overlapping peaks, low intensity and overall a rather high grid size, as discussed in the main part of the paper.

Table S.1. *FWHM of the Gaussian fits of the first three peaks in the spherical integration of the total scattering structure function* $S(\mathbf{Q}) - 1$.

peak	Q (Å^{-1})	FWHM (Å^{-1})
111	2.77	0.37(9)
002	3.19	0.32(4)
022	4.47	0.28(4)

Table S.2. *FWHM of the Gaussian fits of the first three peaks in the spherical integration of the txPDF* $G(\mathbf{r})$.

peak	Q (Å)	FWHM (Å)
$0, \frac{1}{2}, \frac{1}{2}$	2.77	0.44(3)
$0, 0, 1$	3.92	0.40(7)
$\frac{1}{2}, \frac{1}{2}, 1$	4.81	0.44(2)

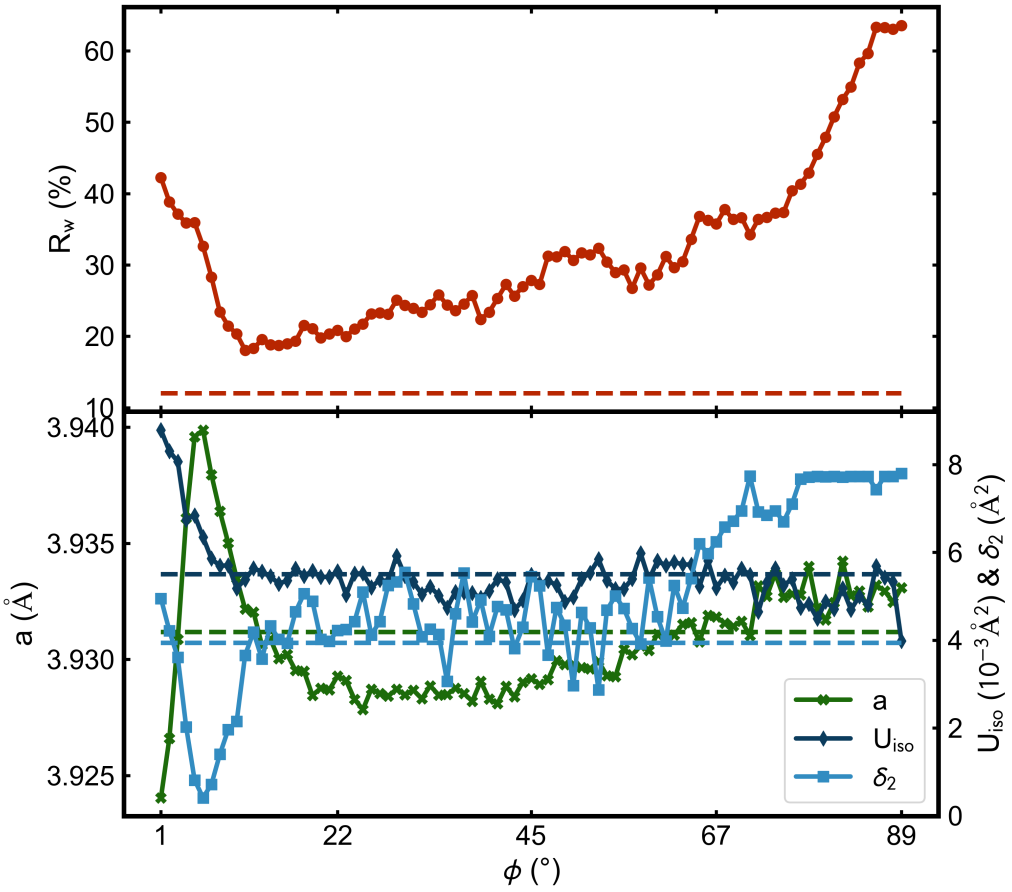

Fig. S.5. PDF refinement results of the 1D PDFs of the Platinum thin film at different tilt angles ϕ. The upper panel shows the goodness of the fit R_w, the lower panel shows the refined structural parameters the lattice parameter, a, the isotropic thermal displacement parameter U_{iso} and the coherent thermal motion parameter δ_2. The dashed line shows the R_w and the refined parameters of the averaged 1D PDF over the whole angular range $\phi = 1°$ to $\phi = 89°$.

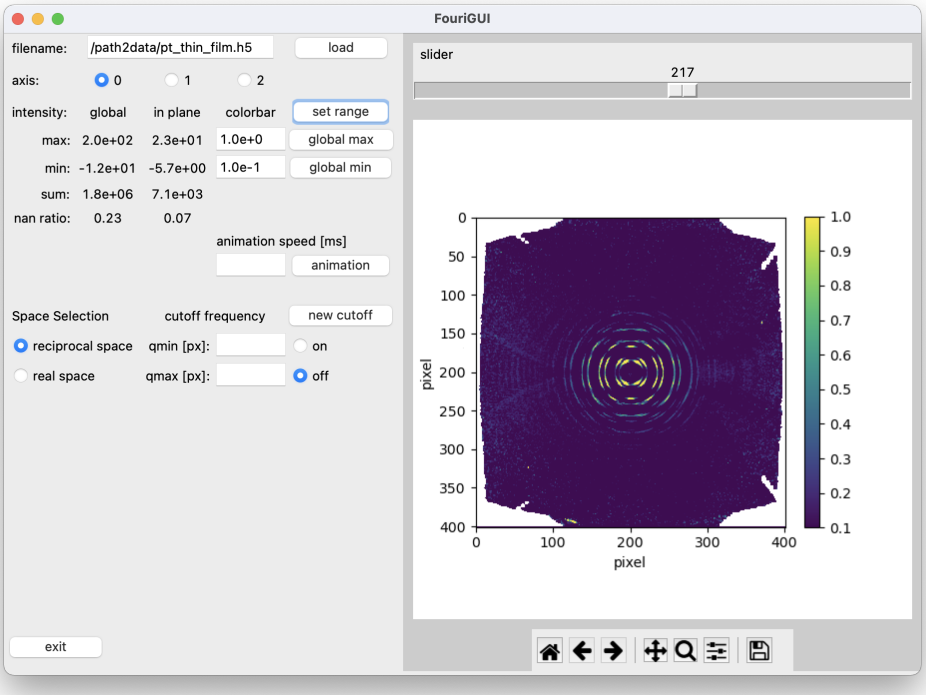

Fig. S.6. Image of FouriGUI in operation with a loaded total scattering structure function $S(\mathbf{Q})$ of the fiber-textured Pt thin film. The data is loaded in h5py file format. FouriGUI displays one plane of the loaded data perpendicular to a specified axis. The slider on the top right enables the user to scroll through the data to visualize slices at different positions along that axis. Fourigui shows global and in-plane live values of the maximum, minimum and summed intensity as well as a measure of the invalid pixels (containing non number values). The Fourier transformation can be performed by changing to real space in the space selection. One can further set cutoff frequencies and evaluate the effect directly in real and reciprocal space. When the animation button is selected, FouriGUI scrolls through the images down the selected axis automatically.

Table S.3. *Applied symmetry operations. The Pt thin film exhibits a strong fiber texture. I.e. it exhibits rotational symmetry about the fiber axis. One can thus perform all symmetry operations about the fiber axis. These can be derived from the reciprocal crystal structure from fcc Pt which is bcc. The symmetrization is done by individually applying the listed symmetry operations to the scattering volume and averaging over these scattering volumes. The inversion center is the origin of the scattering volume. The rotations are performed about the 111-fiber axis, i.e. the z_s axis. The last column names the symmetry operation by the Schönfließ notation.*

#	inversion	rotation	Schönfließ
1	×	0°	1
2	×	120°	C_3
3	×	240°	$2C_3$
4	✓	0°	i
5	✓	120°	$i * C_3$
6	✓	240°	$i * 2C_3$

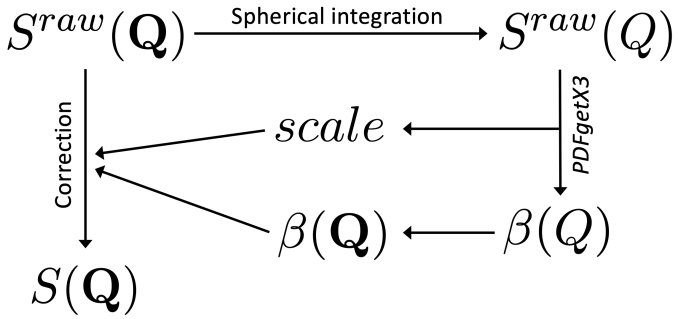

Fig. S.7. Schematic of the applied rescaling and correction procedure to correct for parasitic scattering contributions. We call the uncorrected total scattering structure function which is obtained by dividing the reconstructed scattering volume by the compositional average of the form factors squared (eq. 4) $S^{raw}(\mathbf{Q})$. First, $S^{raw}(\mathbf{Q})$ is spherically integrated from 3D to the 1D uncorrected scattering function $S^{raw}(Q)$. By propagating $S^{raw}(Q)$ through the *PDFgetX3* algorithm one can retrieve the correction term $\beta(Q)$ and the rescaling factor. $\beta(Q)$ produces a slowly changing background that increases in Q. The algorithm estimates the background by fitting a polynomial function to $S^{raw}(Q)$. Please see reference (Juhas *et al.*, 2013) for further details of the *PDFgetX3* algorithm. $\beta(Q)$ models the parasitic scattering contributions. To apply them to $S^{raw}(\mathbf{Q})$, $\beta(Q)$ is isotropically expanded from 1D to 3D to $\beta(\mathbf{Q})$. The corrected scattering function $S(\mathbf{Q})$ is obtained by subtracting $\beta(\mathbf{Q})$ from $S^{raw}(\mathbf{Q})$ and further multiplied with the rescaling factor.

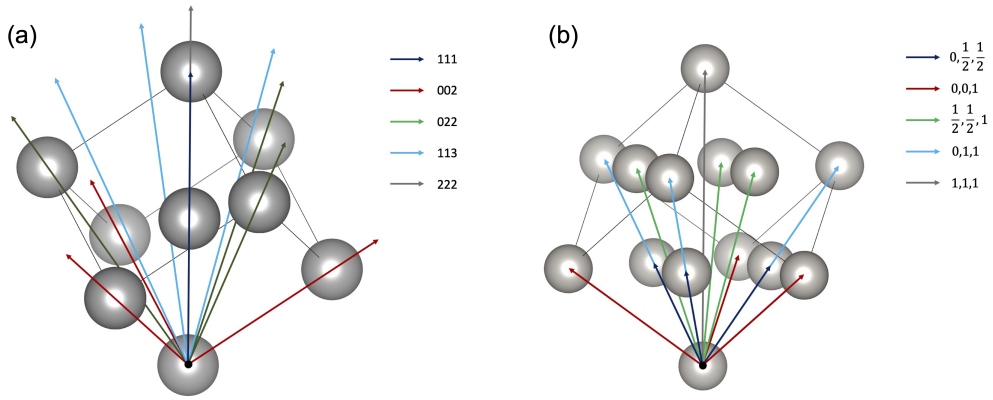

Fig. S.8. Visualization of the directions of the fitted Bragg reflections in reciprocal space (a) and the fitted interatomic vectors in real space (b) for the reciprocal and real space fiber plots, respectively. In terms of clarity, only the directions/interatomic vectors within one unit cell are shown, i.e. the direction/interatomic vector when the zenith angle is smaller than the angle between the 111 and 100 axis. (a) shows the unit cell of the reciprocal structure, base centered cubic (bcc), (b) shows the real space structure, face centered cubic (fcc), of Platinum. Both unit cells are vertically aligned with respect to the 111 fiber axis, $\theta \leq \angle(111, 100) = 54.7°$. In (b) the first five interatomic distances are shown. In (a) the directions to the first five reciprocal lattice points, which correspond to a Bragg reflection are shown. These first reciprocal lattice point exceed the dimensions of one reciprocal unit cell except the 111 lattice point. The Platinum fcc structure only allows Bragg reflection when h,k,l are all even or all odd. Except the 111 lattice point, the lattice points within one reciprocal unit cell correspond to "forbidden" Bragg reflections.

Ashiotis, G., Deschildre, A., Nawaz, Z., Wright, J. P., Karkoulis, D., Picca, F. E. & Kieffer, J. (2015). *Journal of Applied Crystallography*, **48**(2), 510–519. https://doi.org/10.1107/S1600576715004306

Bunge, H. (1982). *Texture Analysis in Materials Science*, vol. 1. Butterworth & Co.

Cervellino, A. & Frison, R. (2020). *Acta Crystallographica Section A Foundations and Advances*, **76**(3), 302–317. http://scripts.iucr.org/cgi-bin/paper?S2053273320002521

Dippel, A.-C., Gutowski, O., Klemeyer, L., Boettger, U., Berg, F., Schneller, T., Hardtdegen, A., Aussen, S., Hoffmann-Eifert, S. & Zimmermann, M. v. (2020). *Nanoscale*, **12**(24), 13103–13112. http://xlink.rsc.org/?DOI=D0NR01847C

Dippel, A.-C., Roelsgaard, M., Boettger, U., Schneller, T., Gutowski, O. & Ruett, U. (2019). *IUCrJ*, **6**(2), 290–298. https://doi.org/10.1107/S2052252519000514

Dosch, H., (1992). Critical phenomena at surfaces and interfaces: Evanescent X-Ray and neutron scattering. ISBN: 9783540384564 OCLC: 801036578.

Egami, T. & Billinge, S. (2012). *Underneath the Bragg Peaks: Structural Analysis of Complex Materials*, vol. 16. Elsevier Science.
https://books.google.de/books?id=kzeSEdYS54wC

Estermann, M. A. & Steurer, W. (1998). *Phase Transitions*, **67**(1), 165–195.
http://www.tandfonline.com/doi/abs/10.1080/01411599808219193

Farrow, C. L., Juhas, P., Liu, J. W., Bryndin, D., Božin, E. S., Bloch, J., Proffen, T. & Billinge, S. J. L. (2007). *Journal of Physics: Condensed Matter*, **19**(33), 335219.
https://iopscience.iop.org/article/10.1088/0953-8984/19/33/335219

Feidenhans'l, R. (1989). *Surface Science Reports*, **10**(3), 105–188.
https://www.sciencedirect.com/science/article/pii/0167572989900022

Gilmore, C. J., K. J. A. & Schenk, H. (2019). *International Tables for Crystallography Vol. H: Powder diffraction*, vol. 1. WILEY.
https://it.iucr.org/H/

Gong, Z. & Billinge, S. J. L. (2018). *arXiv:1805.10342 [cond-mat]*. ArXiv: 1805.10342.
http://arxiv.org/abs/1805.10342

Grote, L., Zito, C. A., Frank, K., Dippel, A.-C., Reisbeck, P., Pitala, K., Kvashnina, K. O., Bauters, S., Detlefs, B., Ivashko, O., Pandit, P., Rebber, M., Harouna-Mayer, S. Y., Nickel, B. & Koziej, D. (2021). *Nature Communications*, **12**(1), 4429.
http://www.nature.com/articles/s41467-021-24557-z

Guo, W., Dmowski, W., Noh, J.-Y., Rack, P., Liaw, P. K. & Egami, T. (2013). *Metallurgical and Materials Transactions A*, **44**(5), 1994–1997.
http://link.springer.com/10.1007/s11661-012-1474-0

Gustafson, J., Shipilin, M., Zhang, C., Stierle, A., Hejral, U., Ruett, U., Gutowski, O., Carlsson, P.-A., Skoglundh, M. & Lundgren, E. (2014). *Science*, **343**(6172), 758–761.
https://www.sciencemag.org/lookup/doi/10.1126/science.1246834

He, B. B. (2018). *Two-dimensional x-ray diffraction*. Hoboken, NJ: John Wiley & Sons, second edition ed.

Hu, E., Li, Q., Wang, X., Meng, F., Liu, J., Zhang, J.-N., Page, K., Xu, W., Gu, L., Xiao, R., Li, H., Huang, X., Chen, L., Yang, W., Yu, X. & Yang, X.-Q. (2021). *Joule*, **5**(3), 720–736.
https://www.sciencedirect.com/science/article/pii/S2542435121000374

Juhas, P., Davis, T., Farrow, C. & Billinge, S. (2013). *Journal of Applied Crystallography*, **46**(2), 560–566.
http://scripts.iucr.org/cgi-bin/paper?S0021889813005190

Kabsch, W. (2010). *Acta Crystallographica Section D Biological Crystallography*, **66**(2), 125–132.
http://scripts.iucr.org/cgi-bin/paper?S0907444909047337

Krogstad, M. J., Rosenkranz, S., Wozniak, J. M., Jennings, G., Ruff, J. P. C., Vaughey, J. T. & Osborn, R. (2020). *Nature Materials*, **19**(1), 63–68.
http://www.nature.com/articles/s41563-019-0500-7

Roelsgaard, M., Dippel, A.-C., Borup, K. A., Nielsen, I. G., Broge, N. L. N., Röh, J. T., Gutowski, O. & Iversen, B. B. (2019). *IUCrJ*, **6**(2), 299–304.
https://doi.org/10.1107/S2052252519001192

Shan, X., Guo, F., Page, K., Neuefeind, J. C., Ravel, B., Abeykoon, A. M. M., Kwon, G., Olds, D., Su, D. & Teng, X. (2019). *Chemistry of Materials*, **31**(21), 8774–8786. Publisher: American Chemical Society.
https://doi.org/10.1021/acs.chemmater.9b02568

Simonov, A., (2019). meerkat.
https://github.com/aglie/meerkat

Song, L., Roelsgaard, M., Blichfeld, A. B., Dippel, A.-C., Jensen, K. M. Ø., Zhang, J. & Iversen, B. B. (2021). *IUCrJ*, **8**(3), 444–454.
https://doi.org/10.1107/S2052252521002852

Weber, T. & Simonov, A. (2012). *Zeitschrift für Kristallographie*, **227**(5), 238–247.
http://www.degruyter.com/doi/10.1524/zkri.2012.1504

Yang, X., Masadeh, A. S., McBride, J. R., Božin, E. S., Rosenthal, S. J. & Billinge, S. J. L. (2013). *Physical Chemistry Chemical Physics*, **15**(22), 8480.
http://xlink.rsc.org/?DOI=c3cp00111c